

Determining the effective width of composite beams with precast hollowcore slabs

Ehab El-Lobody†

Department of Structural Engineering, Faculty of Engineering, Tanta University, Tanta, Egypt

Dennis Lam‡

School of Civil Engineering, University of Leeds, Leeds, LS2 9JT, U.K.

(Received October 8, 2004, Accepted July 7, 2005)

Abstract. This paper evaluates the effective width of composite steel beams with precast hollowcore slabs numerically using the finite element method. A parametric study, carried out on 27 beams with different steel cross sections, hollowcore unit depths and spans, is presented. The effective width of the slab is predicted for both the elastic and plastic ranges. 8-node three-dimensional solid elements are used to model the composite beam components. The material non-linearity of all the components is taken into consideration. The non-linear load-slip characteristics of the headed shear stud connectors are included in the analysis. The moment-deflection behaviour of the composite beams, the ultimate moment capacity and the modes of failure are also presented. Finally, the ultimate moment capacity of the beams evaluated using the present FE analysis was compared with the results calculated using the rigid – plastic method.

Key words: effective width; precast; hollowcore slabs; finite element; modelling; composite design; steel; concrete.

1. Introduction

Composite construction using precast hollowcore units (hcu) is relatively new. For this type of composite beam, mechanical shear connectors pre-welded on to the top flange of the steel beam are used to connect the steel beam with the precast hcu floor. The present knowledge concerning the behaviour of stud connectors within precast hollow core slabs and designing of composite beams with precast hcu slabs is limited (Lam *et al.* 2000a, b). Detailed finite element (FE) analysis of the behaviour of headed stud shear connectors in this form of construction is previously investigated by El-Lobody and Lam (2002) to establish the load-slip behaviour of the headed shear connectors.

In composite design, determination of the effective width (b_{eff}) is traditionally treated by an approximate method. T-section is formed by assuming the steel beam act compositely with an effective width of the concrete slab; usually related to the span of the beam so that simple beam theory can be applied for the analysis. The effective width is typically prescribed in codes of

† Lecturer

‡ Senior Lecturer, Corresponding author, E-mail: d.lam@leeds.ac.uk

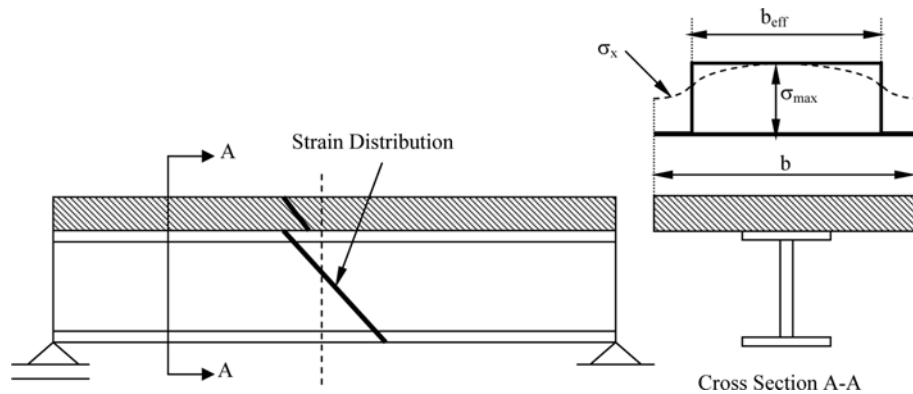


Fig. 1 Definition of effective width for composite beam

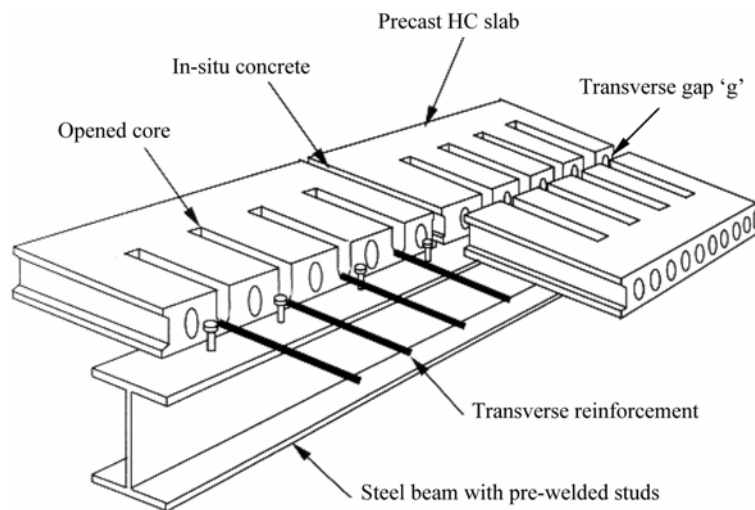


Fig. 2 Composite beam with square-ended hollow core slabs

practice like the EC4 (1994) as the lesser of the distances between parallel beams or one quarter of the effective beam span whichever is the lesser, the same effective width is used for both the elastic and plastic analysis. It is assumed that over the effective width, the strain distribution is kept constant as shown in Fig. 1. This approximation may be true in the elastic stage but may lead to overestimate the effective width at the plastic stage since the effect of concrete cracking and plastic behaviour of steel beam is neglected.

Previous research to evaluate the effective width in composite beams with solid slabs has been carried out by Ansourian (1975), Heins and Fan (1976) and Amadio and Fragiaco (2002), but no work has been carried out to determine the effective width for composite beams with precast hollowcore slabs. The effective width for composite beams with hollowcore slabs is complicated due to the presence of the in-situ and precast concrete, as well as the presence of the hollow cores (see Fig. 2). In this paper, finite element method previously developed by El-Lobody and Lam (2003) is used to carry out parametric study to establish the effective slab width for this form of composite slabs. Beams with different spans (6 m, 9 m and 12 m), hollowcore units' depth

(150 mm, 200 mm and 250 mm) and steel sections (UB 356, UB 406 and UB 457) were used for this study. The material non-linearity of precast concrete, in-situ concrete and the steel beams are taken into account. The load-slip characteristic of the shear connectors are taken from the previous finite element analyses by El-Lobody and Lam (2002).

2. Modelling of composite beams with precast hollowcore slabs

The composite beams modelled in this research, consists of steel beam, pre-welded headed stud shear connectors, prestressed hcu's and cast in-situ concrete. The hcus' are rested directly on the top flange of the steel beam, with an in-situ gap 'g' in the longitudinal direction as shown in Fig. 2. The alternative cores of each hcu were left open for a length of 500 mm to allow for placing of the transverse reinforcement. Fig. 3 shows a standard 1200 mm width \times 150 mm depth precast hollow core unit. Reinforcing bar is placed on site into the open cores and filled with a minimum grade C25 in-situ concrete. Fig. 4 shows the section of the precast / in-situ joint of the composite beam with hollowcore slabs. The longitudinal and transverse joints between the hcus' are filled with in-situ concrete so that horizontal compressive forces can be transferred through the slabs.

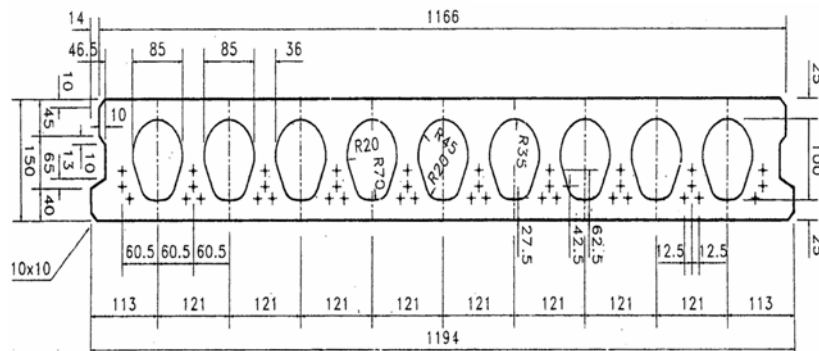


Fig. 3 Details of a typical 1200 mm length hollow core unit

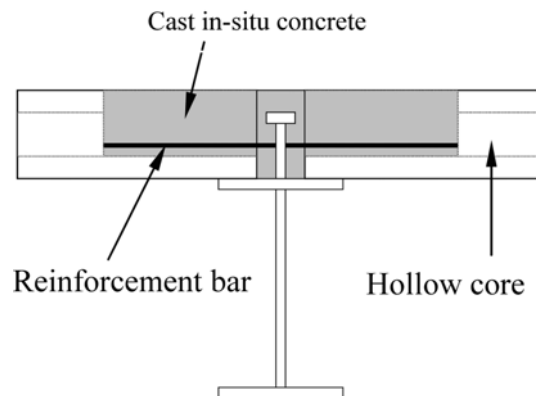


Fig. 4 Details of the precast-in-situ joint of composite beam with square-end hollowcore slabs

2.1 Finite element mesh and boundary conditions

The three-dimensional FE solid elements are used to model the composite beams. Each precast unit is modelled with 114 elements. The in-situ concrete infill is modelled with 160 elements for the 6 m span beam; 240 elements for the 9 m span beam and 320 elements for the 12 m span beam. The in-situ infill which contained the reinforcing bar is modelled with 1 element in the x -direction, 2 elements in the y -direction and 1 element in the z -direction. Fig. 5 shows the 3-D FE model of the composite beams used in this study. For the boundary conditions, all nodes of precast concrete units, in-situ concrete and the steel beam in the symmetry surface passing through the middle of

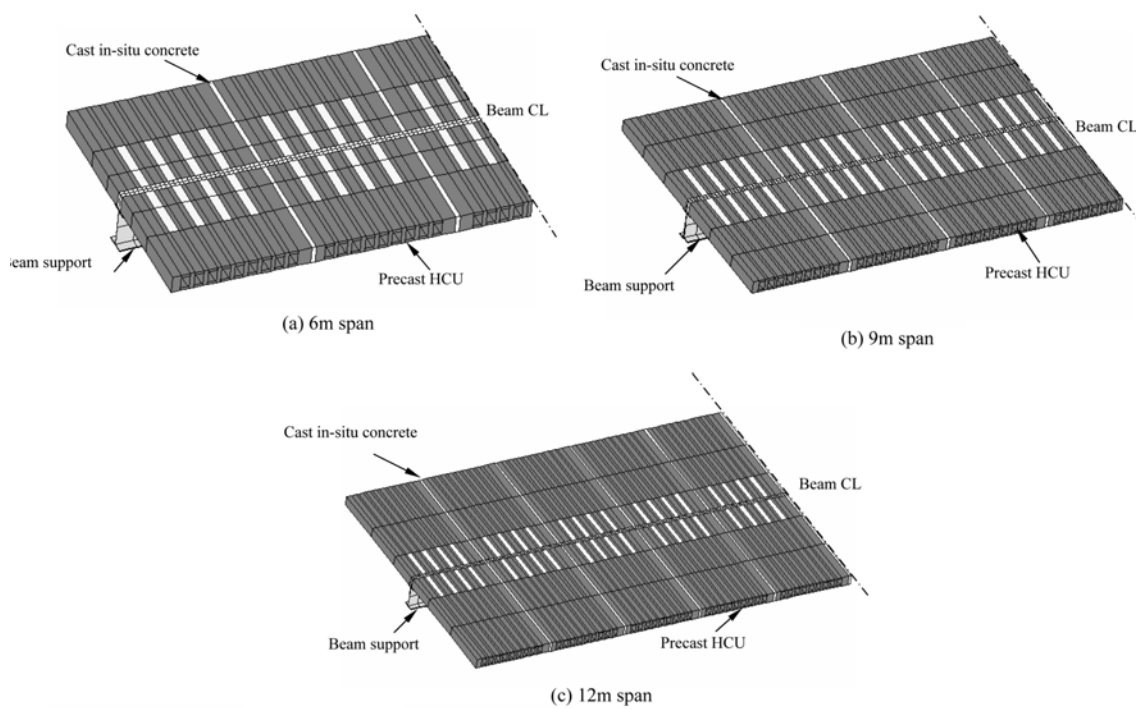


Fig. 5 FE mesh of composite beams with precast hollowcore slabs

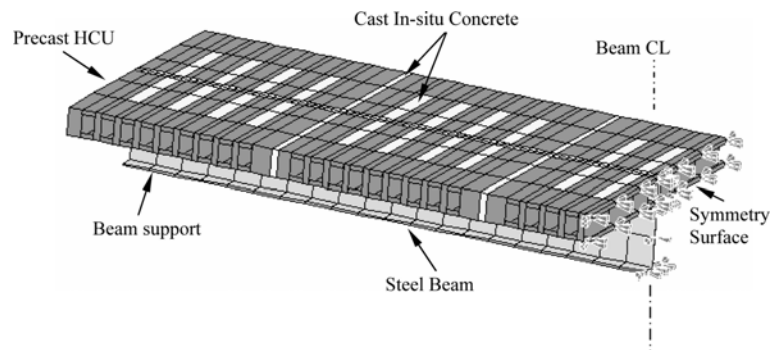


Fig. 6 Boundary conditions for the composite beam

beams are restricted to move in the x - and y -directions as shown in Fig. 6. The support is allowed to move in the x -direction but prevented to move in the y - and z -directions. The load is applied as uniformly distributed load using the RIKS method available from the ABAQUS (1998).

2.2 Concrete material model

Modelling of the concrete elements is the most important part of this study. Concrete is assumed to be an isotropic material prior to cracking. The presence of cracks affects the stress and material stiffness of the elements.

2.2.1 Concrete cracking

Concrete cracking is the most important aspect in modelling the concrete elements and representation of cracks and post-cracking behaviour dominates the accuracy of the model. Cracking is occurred when the stress reached a failure surface, which is called “crack detection surface”. This failure surface is a linear relationship between the equivalent pressure stress, p and the *Von Mises* equivalent stress, q . Once a crack has been detected, its orientation is stored and subsequent cracking at the same point is assumed to be orthogonal to this direction. The post failure behaviour of direct straining across cracks is modelled with the *TENSION STIFFENING option in ABAQUS (1998).

2.2.2 Tensile and compressive behaviour

Concrete in tension is considered as linear-elastic material until the uni-axial tensile stress, f_t . A linear softening model is assumed to represent the post-failure behaviour in tension by tension stiffening, this allows for the effects of interaction between reinforcement and concrete. Concrete in compression is considered to be a linear-elastic / plastic material. When the principal stress components are dominantly compressive, the response of concrete is modelled by elastic-plastic

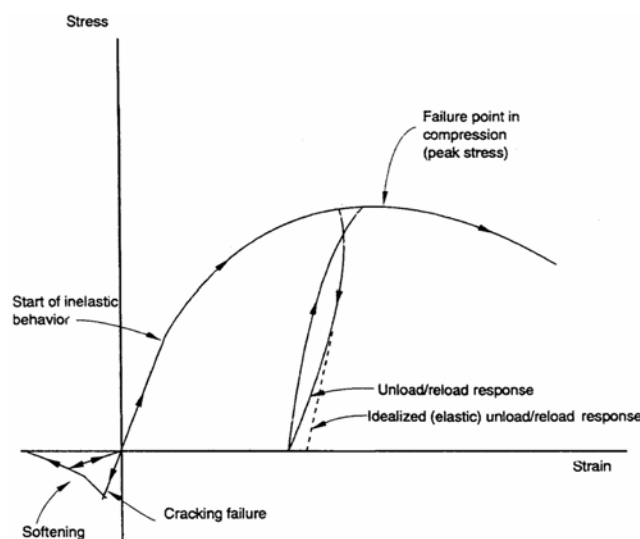


Fig. 7 Uni-axial behaviour of plain concrete

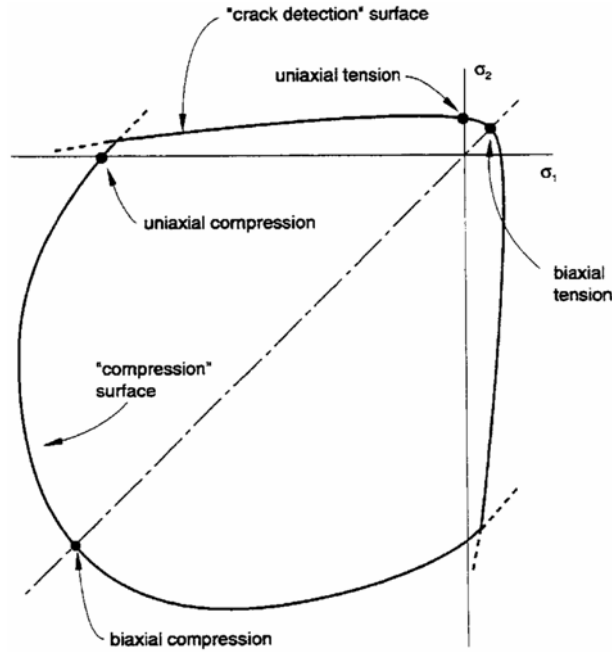


Fig. 8 Yield and failure surface for in-plane stresses

theory using a simple form of yield surface. This surface is written in terms of the equivalent pressure stress, p , and the *Von Mises* equivalent stress, q . The cracking and compressive responses of concrete that are incorporated in the model are illustrated by the uni-axial behaviour shown in Fig. 7. When concrete is loaded in compression, it initially exhibits elastic response. As the stress is increased, some inelastic straining occurs and the response of the material softens. When ultimate stress ' f_{uc} ' is reached, the material start to lose the strength until it can no longer carry any stress. In multi-axial stress states these observations are generalised through the concept of surfaces of failure and flow in stress space. These surfaces are fitted to experimental data as shown in Fig. 8.

Following the BS8110 (1997), average values of ultimate strain at failure ' ϵ_u ', the ultimate compression stress of concrete ' f_{uc} ', the initial Young's modulus ' E_{co} ' can be calculated from the following relations:

$$\epsilon_u = 0.00024 \sqrt{f_{cu}} \quad (1)$$

$$f_{uc} = 0.67 f_{cu} \quad (2)$$

$$E_{co} = 5500 \sqrt{f_{cu}} \quad (3)$$

2.3 Steel material model

The steel material in this study is treated as elastic – plastic material, i.e., it behaves linear elastically up to the yield stress of steel, f_{ys} , see Fig. 9. After this stage it becomes fully plastic. In the present study, E_s is taken as 200000 N/mm² and f_{ys} is taken as 275 N/mm².

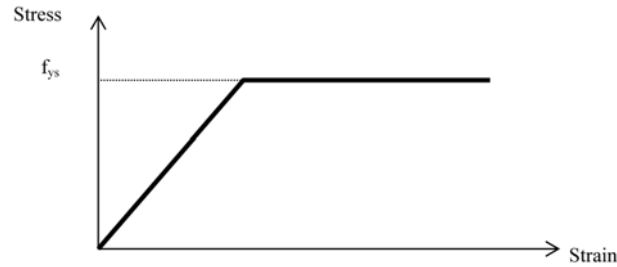


Fig. 9 Bilinear stress-strain curve for steel (elastic-plastic model)

2.4 Modelling of reinforcing bars

Transverse reinforcement embedded in the slabs is defined by using the *REBAR option in ABAQUS. It is defined as individual reinforcing bars in the elements with an area equivalent to the cross section area of the reinforcement bar. The material properties of the bars are distinct from those of the underlying elements and are defined separately. In this present study, a similar bilinear curve as shown in Fig. 9 for steel section is used in modelling the reinforcing bar with a yield stress f_{ys} taken as 460 N/mm^2 .

2.5 Modelling of headed stud shear connectors

In a composite steel and concrete beam, shear connectors are provided throughout the length of the beam to transmit the longitudinal shear force between the steel beam and the concrete slabs. The shear connector is modelled and defined in this model as non-linear spring element. The spring element is of zero length that carried the shear force, and obeyed the load-slip characteristic of the shear connector used. The positions of the spring elements are coincided with the positions of the shear connectors used in the composite beam. Because the load-slip characteristic of the shear connector is non-linear, the force is a function of relative displacement in the spring. The load-slip characteristic of the shear connector is obtained from the corresponding FE-model previously developed by El-Lobody and Lam (2002).

3. Effective width for elastic and plastic analysis

3.1 Effective width for elastic analysis

In elastic analysis, the effective width of the slab b_{eff} is theoretically defined as the width of slab that develops the actual total horizontal force in the slab when the stress is assumed constant at the peak value and this can be represented mathematically by:

$$b_{eff} = \frac{\int_{-b/2}^{b/2} \sigma_x dy}{\sigma_{max}} \quad (4)$$

In a non-linear step-by-step incremental load procedure, the stresses and strains at the end of the first increment are obtained based on elastic material properties. So, by integrating the longitudinal axial stresses over the width 'b' at the end of the first increment and dividing the result by the peak value of the longitudinal stress, the elastic effective width can be calculated easily. This approach is used in this present parametric study to evaluate the elastic effective width of composite beams with precast hollowcore slabs.

3.2 Effective width for plastic analysis

The elasto-plastic analysis of composite beams was accomplished by a step-by-step load incremental procedure. Initially, the composite beam is solved by an elastic analysis and the stresses at the end of the first increment are calculated. The minimum value of the load that will cause any point in the structure to yield is determined. The elastic equations are then modified so that the equations at the yield points obeyed the plastic condition. Loads are then applied to the structure in increments to form additional yield points. For each load increment, it is necessary to solve the equilibrium equations and to find the distribution of incremental stresses in equilibrium with the increments of loads. Therefore, at any load stage, the internal stress field will always satisfy the equations of equilibrium and the yield condition, together with the boundary conditions. The procedure is repeated until the yielding has spread to a stage when equilibrium may no longer be maintained or convergence during the iteration procedure can no longer be obtained. *Von Mises'* yield criteria govern the equilibrium at the plastic stage of the composite beams.

When the slabs in the composite beams reached plasticity, normal stress became uniform along the width of the cross section. The theoretical effective width, calculated from Eq. (4), will cover the part that has uniform normal stress (maximum uni-axial compressive stress), in addition to the parts that represent the transfer of stresses from the yielded section to the non-yielded section, see Fig. 10. Due to cracking of the concrete, the transfer of stresses from the cracked sections to the uncracked sections can not be guaranteed. So, for design safety, the plastic effective width in this

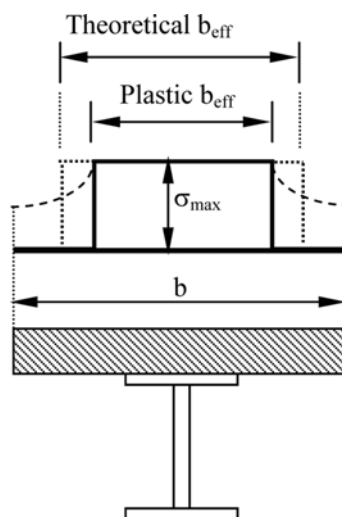


Fig. 10 Definition of the plastic effective width of the composite beam

study will be considered as the width that has uniform maximum longitudinal axial stress over the width of the cross section at failure. Unlike the elastic effective width, the plastic effective width is dependent to the material properties of the composite beam's components.

4. Parametric study of the effective width

Twenty-seven composite beams with precast hollowcore slabs were analysed in the parametric study as shown in Table 1. The FE model used is previously validated against the experimental data and presented in El-Lobody and Lam (2003). The beams are loaded with uniformly distributed load up to failure and the distribution of longitudinal axial stresses is plotted on the top surface of the concrete slab at failure. All beams are classified into 9 main groups depending on the steel beam

Table 1 Summary of the beams in the parametric study

Group	Beam	Steel Beam Sizes	HCU Depth (mm)	Span (m)
G1	S1	UB 356 × 171 × 51	150	6
	S2	UB 356 × 171 × 51	150	9
	S3	UB 356 × 171 × 51	150	12
G2	S4	UB 406 × 178 × 60	150	6
	S5	UB 406 × 178 × 60	150	9
	S6	UB 406 × 178 × 60	150	12
G3	S7	UB 457 × 191 × 67	150	6
	S8	UB 457 × 191 × 67	150	9
	S9	UB 457 × 191 × 67	150	12
G4	S10	UB 356 × 171 × 51	200	6
	S11	UB 356 × 171 × 51	200	9
	S12	UB 356 × 171 × 51	200	12
G5	S13	UB 406 × 178 × 60	200	6
	S14	UB 406 × 178 × 60	200	9
	S15	UB 406 × 178 × 60	200	12
G6	S16	UB 457 × 191 × 67	200	6
	S17	UB 457 × 191 × 67	200	9
	S18	UB 457 × 191 × 67	200	12
G7	S19	UB 356 × 171 × 51	250	6
	S20	UB 356 × 171 × 51	250	9
	S21	UB 356 × 171 × 51	250	12
G8	S22	UB 406 × 178 × 60	250	6
	S23	UB 406 × 178 × 60	250	9
	S24	UB 406 × 178 × 60	250	12
G9	S25	UB 457 × 191 × 67	250	6
	S26	UB 457 × 191 × 67	250	9
	S27	UB 457 × 191 × 67	250	12

cross section and the precast hollowcore unit used. Each group contains three different beam spans of 6, 9 and 12 m and has the same steel cross section and the same hcu's depth. The width of the concrete slab is chosen so that the ratio of the slab width 'b' to the beam span 'L' remains constant. The b/L ratio is chosen to be approximately equal to 0.3 and the effect to the ratio on the calculation of the effective width will be discussed later. The width of the concrete slab is taken as 2065 mm (1000 mm hcu's width each side + 65 mm gap width between hcus) for the 6 m span beams, 3065 mm (1500 mm hcu's width each side + 65 mm gap width between hcus) for the 9 m span beams and 4065 mm (2000 mm hcu's width each side + 65 mm gap width between hcus) for the 12 m span beams.

The hcu has characteristic cube strength of 50 N/mm^2 while the cast in-situ concrete has a concrete strength of 26 N/mm^2 . The steel beam has a yield stress of 275 N/mm^2 . 10 mm transverse reinforcing bars are used for all the 27 beams. The load-slip characteristic of the 19 mm diameter \times 100 mm height used with hcu concrete slab; 26 N/mm^2 cast in-situ concrete and 10 mm transverse reinforcement is taken from the previous FE study by El-Lobody and Lam (2002).

The approach adopted to evaluate the elastic effective width (the effective width calculated base on elastic material properties) and the plastic effective width (the effective width calculated base on elastic-plastic material properties) is as previously discussed. The procedures are explained here for group G1 and applied for the other eight groups carried out in this parametric study.

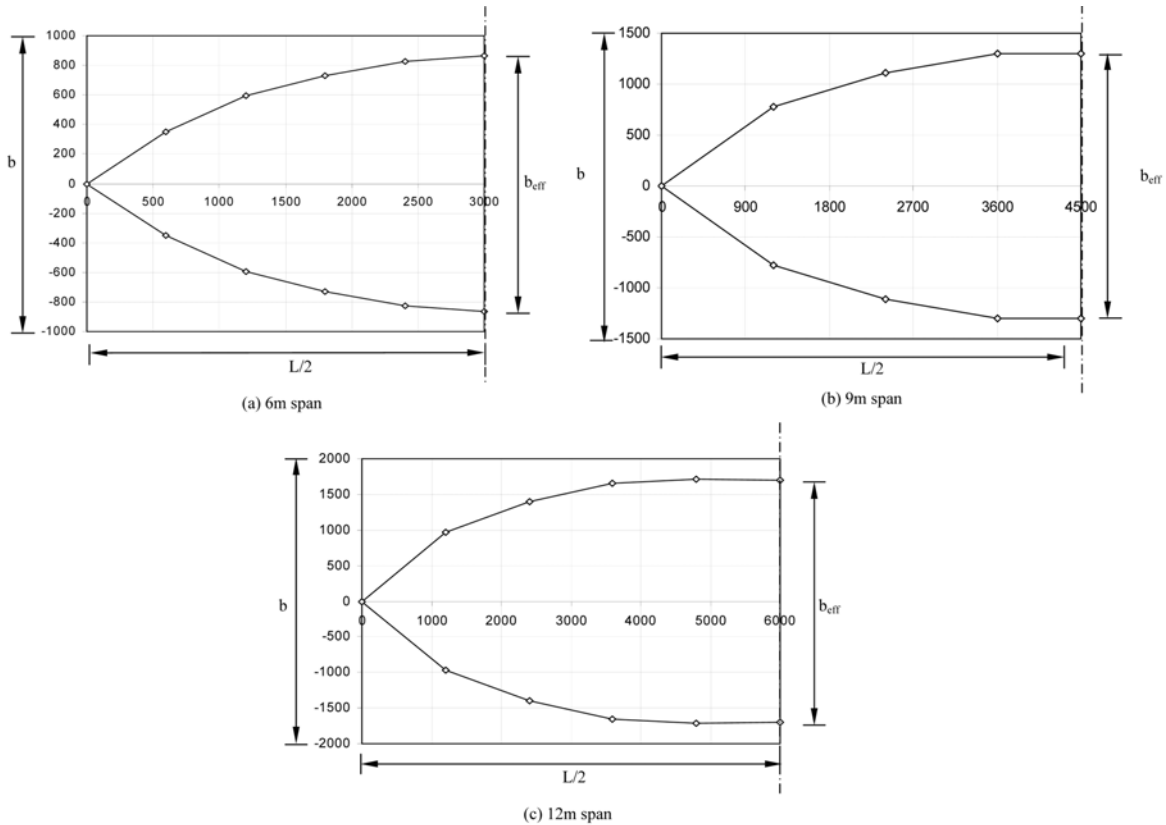


Fig. 11 Distribution of the elastic effective breadth

Table 2 Elastic effective width at cross section of the composite beam

Beam	Steel Beam Sizes	hcu depth (mm)	Span L (m)	Elastic Effective width (mm)						
				.1L	.13L	.2L	.27L	.3L	.4L	.5L
S1	UB 356 × 171 × 51	150	6	700	-	1184	-	1460	1649	1730
S2	UB 356 × 171 × 51	150	9	-	1560	-	2228	-	2598	2598
S3	UB 356 × 171 × 51	150	12	1944	-	2801	-	3310	3418	3406

4.1 Elastic effective width

The stress distribution through the cross section has been plotted at different sections over the span. Since there are different material properties (even in the same section due to the presence of the cast in-situ concrete, precast hollow core slab, and the presence of the hollow cores), the distribution is plotted at each section to obtain the critical effective width value. Integration for the effective width has been carried out numerically using the trapezoidal rule to evaluate the elastic effective width at different sections for the beams (S1, S2 and S3) that spanned 6, 9 and 12 m and have the same (b/L) ratio. Fig. 11 shows the distribution of the elastic effective width over the span for beam S1, S2 and S3 respectively. In addition, Table 2 shows the elastic effective width values at different sections along the length of beams S1, S2 and S3. The elastic (b_{eff}/L) ratio calculated at centre line of the beams for S1, S2 and S3 was approximately the same and equals to 0.288 for b/L ratio equal to 0.34.

4.2 Plastic effective width

Fig. 12 shows the distribution of longitudinal axial stresses at failure on the concrete surface of the composite beams S1, S2 and S3 respectively. Since the critical compressive stress is governed by the in-situ infill concrete strength, the stress contour is taken between -26 N/mm^2 to $+26 \text{ N/mm}^2$. It can be seen that the distribution of axial stress over the section at failure is uniform over the yielded elements of the concrete slab and decreases towards the edges as previously explained. The constant width of the precast hollowcore / in situ concrete slab represents the actual width that interacts with the steel beam in carrying longitudinal axial stresses (plastic effective width). This width remains approximately the same even when greater width of concrete 'b' is used.

Table 3 shows the summary of the plastic effective width calculated at failure of the composite beams S1, S2 and S3 and the remaining eight groups. The average plastic (b_{eff}/L) ratio calculated at centre-line of the beams is 0.237 (for b/L ratio = 0.34), this means that the calculation of the effective width based on elastic material properties may lead to an unsafe value. In order to justify this conclusion, the present parametric study has been carried out over a variety of composite steel-precast hollowcore beams that have different steel cross sections and different hollowcore slab's depth but have the same b/L ratio.

The average elastic effective width / span ratio for all the beams is approximately 0.29 and the average plastic effective width / span ratio for the beams based on ultimate state is approximately 0.22. These values are calculated at the mid – span of the composite beams.

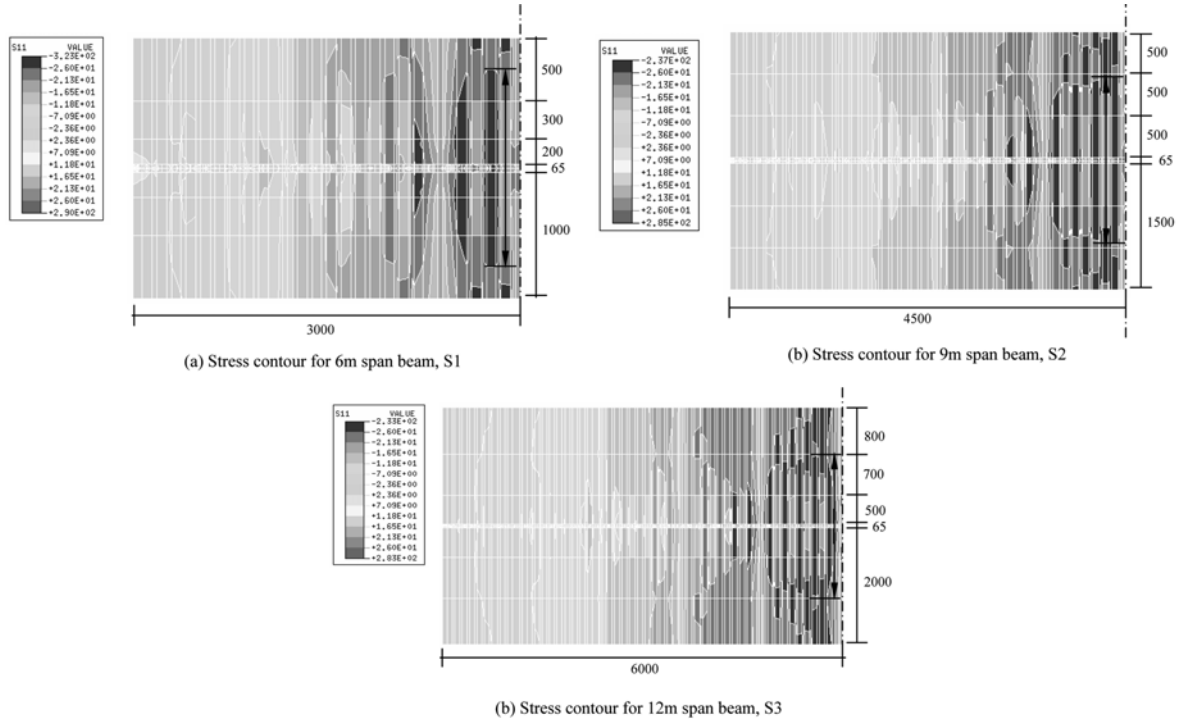
Fig. 12 Stress contour for Group 1 ($356 \times 171 \times 51$ UB, 150 mm deep slabs)

Table 3 Summary of the plastic effective width / span ratio

Group	Beam	Beam span, L (mm)	b_{eff} (mm)	b_{eff}/L (mm)
G1	S1	6000	1692	0.282
	S2	9000	2008	0.223
	S3	12000	2465	0.205
G2	S4	6000	1591	0.265
	S5	9000	2065	0.229
	S6	12000	2465	0.205
G3	S7	6000	1557	0.259
	S8	9000	2065	0.229
	S9	12000	2465	0.205
G4	S10	6000	1557	0.259
	S11	9000	1800	0.200
	S12	12000	2258	0.188
G5	S13	6000	1502	0.25
	S14	9000	2065	0.229
	S15	12000	2465	0.205

Table 3 Continued

Group	Beam	Beam span, L (mm)	b_{eff} (mm)	b_{eff}/L (mm)
G6	S16	6000	1620	0.27
	S17	9000	1964	0.218
	S18	12000	2465	0.205
G7	S19	6000	1490	0.248
	S20	9000	1792	0.199
	S21	12000	1516	0.126
G8	S22	6000	1475	0.246
	S23	9000	2028	0.225
	S24	12000	2098	0.175
G9	S25	6000	1452	0.242
	S26	9000	1950	0.217
	S27	12000	2064	0.172

4.3 Effect of 'b/L' ratio on the calculation of effective width

The parametric study on a variety of composite beams with hollowcore slabs has shown that, for a 'b/L' ratio equals to 0.34, the effective width calculated based on elastic material properties is greater than that one calculated based on elastic-plastic material properties. To investigate the effect of 'b/L' ratio on the effective width, parametric study has been extended to calculate the elastic and plastic effective widths at different b/L ratios. The 9 m span beam 'S2' is analysed using the same procedures used but with different b/L ratios. Fig. 13 shows the relationship between 'b_{eff}/L' and 'b/L' ratios. It can be seen that both the elastic effective width and the plastic

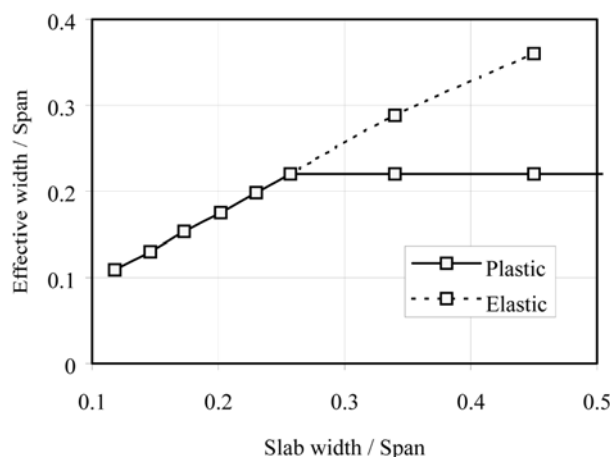


Fig. 13 Effective width of composite steel-precast HC slab girders

effective width are increased with the increase of the slab width until the plastic effective width reaches a constant value. The average value of the effective width is equal to $0.22L$ for all of the beams that has $b \geq 0.26L$. This value is calculated at the mid – span and decreases towards the support as shown in Fig. 11.

5. Moment-deflection curves for composite beams with precast hollowcore slabs

The effective width obtained from the parametric study was used to attain the moment vs. mid-span deflection curves, ultimate moment capacity and modes of failure for the beams. Fig. 14 shows the moment-deflection curves of composite beams with hollowcore slab's depth of 150 mm and different steel cross sections for 6, 9 and 12 m span respectively. Fig. 15 shows the moment-deflection curves of composite beams with hollowcore slab's depth of 200 mm and Fig. 16 shows the moment-deflection curves of composite beams with hollowcore slab's depth of 250 mm.

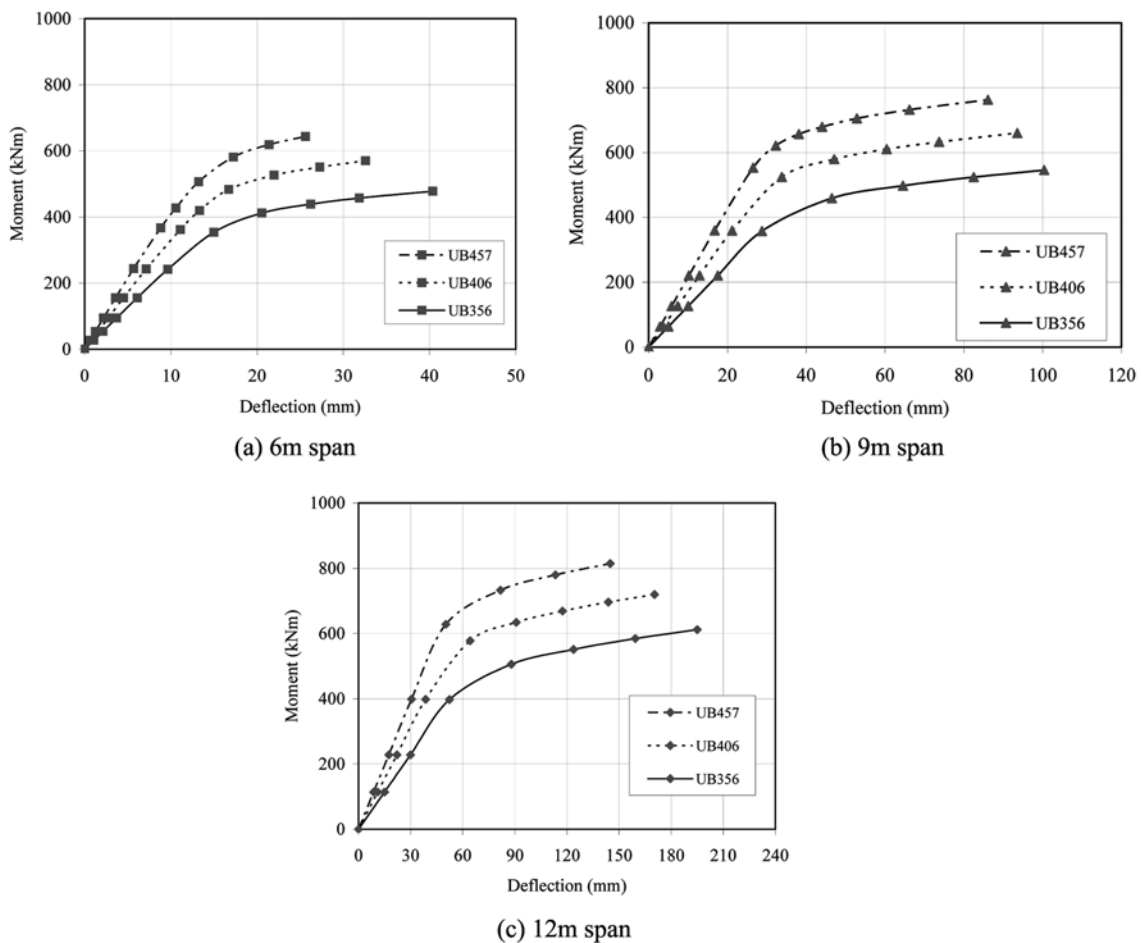


Fig. 14 Moment vs. mid-span deflection curves for 150 mm slabs

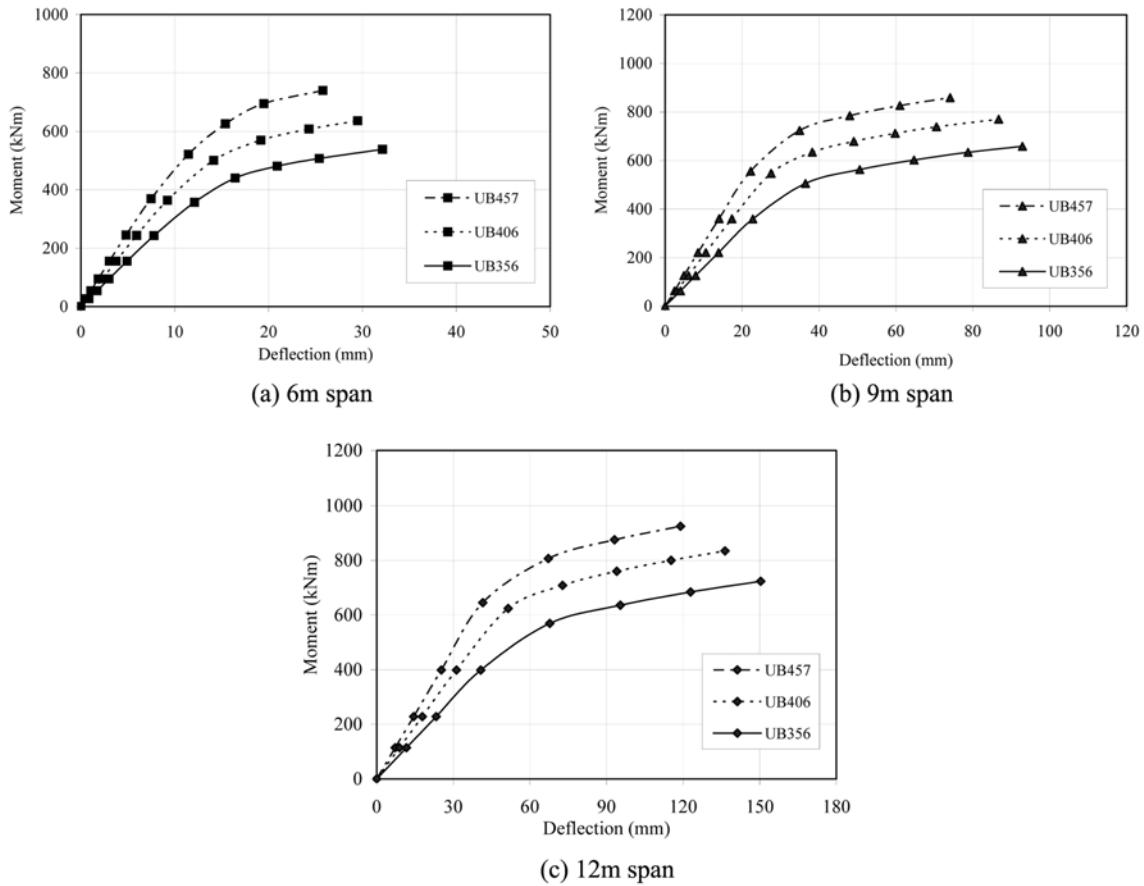


Fig. 15 Moment vs. mid-span deflection curves for 200 mm slabs

Four modes of failure were checked to determine the failure point of composite beams: a) yielding of the steel beam; b) failure of the shear connectors; c) tensile failure of the bottom surface of the concrete slabs and d) compressive failure of top surface of concrete slabs. In general, the elastic neutral axis was closed to the interface between the steel beam and the concrete slab for most of the beams, by increasing the loading beyond the elastic stage; this resulted in yielding of the bottom flange of the steel beam and moving the neutral axis towards the compression zone and hence, inducing tension to the slabs. With the moment further increased, the load carried by the composite section remained constant and the crushing of the concrete slab occurred. Failure of the shear connectors could occur between yielding of the steel beam and crushing of the concrete slabs and resulted in reduction of the load carrying capacity of the composite section. The ductility of the beams decreased with the increase in hcu's depth for the same span and the same steel beam cross section. The moment capacity and flexural stiffness of the composite beams was increased compared to the capacity of the steel beam alone. The ultimate moment capacity of the composite beams obtained from present FE analysis together with modes of failure are summarised in Table 4.

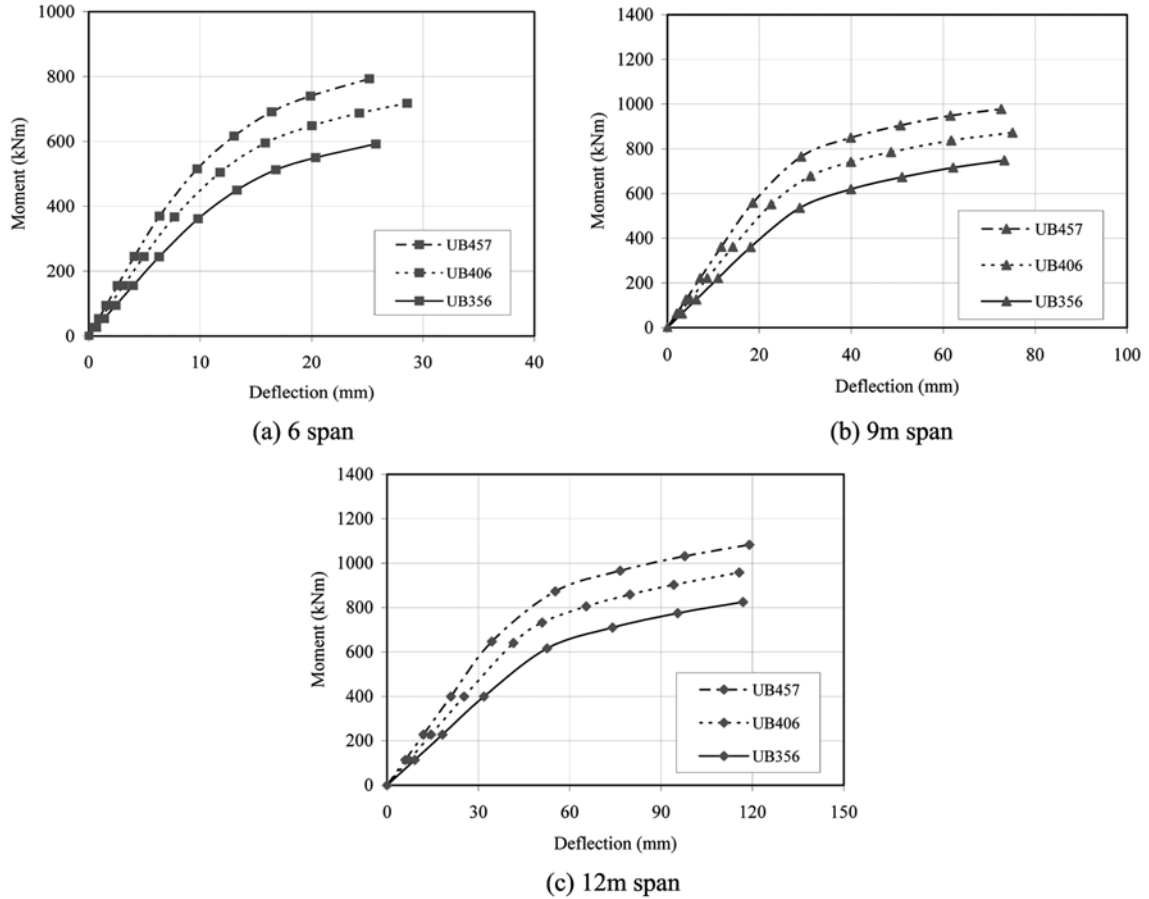


Fig. 16 Moment vs. mid-span deflection curves for 250 mm slabs

6. Calculate moment capacity using rigid – plastic analysis

Following the same approach explained by Lam *et al.* (2000b), the ultimate moment capacity of the beams under investigation can be calculated using rigid – plastic analysis. The concrete slab is assumed to be stressed with a stress equals to $0.45f_{cu}$ over its effective width. The resistance of the concrete flange, F_{conc} is given by:

$$F_{conc} = 0.45f_{cu}b_{eff}d_p \quad (5)$$

Where f_{cu} is the compressive concrete cube strength of the in-situ concrete and is equal to 26 N/mm^2 ; b_{eff} is the effective width determined from the parametric study as 0.22 of the span and d_p is the depth of the slab.

The resistance of the steel beam F_{steel} is given by:

$$F_{steel} = A_{steel}f_{ys} \quad (6)$$

Where A_{steel} is the cross sectional area of the steel beam and f_{ys} is the yield stress of the steel beam

Table 4 Summary of the ultimate moment capacity

Group	Beam	UB	b_{eff} (mm)	d_p (mm)	A_s (cm ²)	D (mm)	T_{flange} (mm)	B_{flange} (mm)	Z_{pl} (cm ³)	M_s (kN.mm)	F_{flange} (kN)	F_{conc} (kN)	F_{steel} (kN)	F_{con} (kN)	Failure Mode	M_{comp} cal. (kN.m)	M_{comp} FE (kN.m)	M_{comp} cal. M_{comp} FE
G1	S1	356×171×51	1320	150	64.9	355	11.5	171.5	896	246400	542.4	2316.6	1784.75	1470	Concrete	396	478	0.83
	S2	356×171×51	1980	150	64.9	355	11.5	171.5	896	246400	542.4	3474.9	1784.75	2170	Concrete	516	546	0.95
	S3	356×171×51	2640	150	64.9	355	11.5	171.5	896	246400	542.4	4633.2	1784.75	2870	Concrete	533	612	0.87
G2	S4	406×178×60	1320	150	76.5	406.4	12.8	177.9	1199	329725	626.2	2316.6	2103.75	1470	Steel beam	478	570	0.84
	S5	406×178×60	1980	150	76.5	406.4	12.8	177.9	1199	329725	626.2	3474.9	2103.75	2170	Steel beam	648	660	0.98
	S6	406×178×60	2640	150	76.5	406.4	12.8	177.9	1199	329725	626.2	4633.2	2103.75	2870	Steel beam	671	720	0.93
G3	S7	457×191×67	1320	150	85.5	453.4	12.7	189.9	1471	404525	663.2	2316.6	2351.25	1470	Steel beam	551	644	0.86
	S8	457×191×67	1980	150	85.5	453.4	12.7	189.9	1471	404525	663.2	3474.9	2351.25	2170	Steel beam	628	763	0.82
	S9	457×191×67	2640	150	85.5	453.4	12.7	189.9	1471	404525	663.2	4633.2	2351.25	2870	Steel beam	796	814	0.98
G4	S10	356×171×51	1320	200	64.9	355	11.5	171.5	896	246400	542.4	3088.8	1784.75	1470	Concrete	469	538	0.87
	S11	356×171×51	1980	200	64.9	355	11.5	171.5	896	246400	542.4	4633.2	1784.75	2170	Concrete	605	658	0.92
	S12	356×171×51	2640	200	64.9	355	11.5	171.5	896	246400	542.4	6177.6	1784.75	2870	Concrete	622	724	0.86
G5	S13	406×178×60	1320	200	76.5	406.4	12.8	177.9	1199	329725	626.2	3088.8	2103.75	1470	Steel beam	552	636	0.87
	S14	406×178×60	1980	200	76.5	406.4	12.8	177.9	1199	329725	626.2	4633.2	2103.75	2170	Steel beam	753	770	0.98
	S15	406×178×60	2640	200	76.5	406.4	12.8	177.9	1199	329725	626.2	6177.6	2103.75	2870	Steel beam	777	835	0.93
G6	S16	457×191×67	1320	200	85.5	453.4	12.7	189.9	1471	404525	663.2	3088.8	2351.25	1470	Stud	625	740	0.84
	S17	457×191×67	1980	200	85.5	453.4	12.7	189.9	1471	404525	663.2	4633.2	2351.25	2170	Stud	737	859	0.86
	S18	457×191×67	2640	200	85.5	453.4	12.7	189.9	1471	404525	663.2	6177.6	2351.25	2870	Stud	914	925	0.99
G7	S19	356×171×51	1320	250	64.9	355	11.5	171.5	896	246400	542.4	3861	1784.75	1470	Concrete	543	592	0.92
	S20	356×171×51	1980	250	64.9	355	11.5	171.5	896	246400	542.4	5791.5	1784.75	2170	Concrete	694	748	0.93
	S21	356×171×51	2640	250	64.9	355	11.5	171.5	896	246400	542.4	7722	1784.75	2870	Concrete	711	825	0.86
G8	S22	406×178×60	1320	250	76.5	406.4	12.8	177.9	1199	329725	626.2	3861	2103.75	1470	Steel beam	625	718	0.87
	S23	406×178×60	1980	250	76.5	406.4	12.8	177.9	1199	329725	626.2	5791.5	2103.75	2170	Steel beam	858	872	0.98
	S24	406×178×60	2640	250	76.5	406.4	12.8	177.9	1199	329725	626.2	7722	2103.75	2870	Steel beam	882	958	0.92
G9	S25	457×191×67	1320	250	85.5	453.4	12.7	189.9	1471	404525	663.2	3861	2351.25	1470	Stud	698	793	0.88
	S26	457×191×67	1980	250	85.5	453.4	12.7	189.9	1471	404525	663.2	5791.5	2351.25	2170	Stud	845	978	0.86
	S27	457×191×67	2640	250	85.5	453.4	12.7	189.9	1471	404525	663.2	7722	2351.25	2870	Stud	1031	1083	0.95

and is equal to 275 N/mm² for structural steel grade S275.

For composite beam with full shear interaction (i.e., sufficient number of shear connectors is used to transfer the longitudinal shear forces at the steel-concrete interface), F_{con} (the resistance force of the shear connectors) is greater than the smaller of F_{conc} or F_{steel} . F_{con} is given by:

$$F_{con} = nP_R \quad (7)$$

Where n is the number of shear connectors spaced at S in a half span $L/2$ ($n = L/2S + 1$) and P_R is the resistance of the shear connector obtained from previous FE analysis by El-Lobody and Lam (2002) and equals to 70 kN for the 19 mm diameter \times 100 mm height headed stud in push-off test with hollowcore slab with in-situ concrete strength of 26 N/mm² and transverse reinforcing bars of 10 mm in diameter.

For a plastic neutral axis in the concrete flange ($F_{conc} > F_{steel}$), the calculated ultimate moment capacity of the composite beam is given by:

$$M_{comp} = F_{steel} \left(\frac{D}{2} + d_p - \frac{F_{steel} d_p}{F_{conc}} \right) \quad (8)$$

For a plastic neutral axis in the steel section ($F_{steel} > F_{conc}$), the calculated ultimate moment capacity of the composite beam is given by:

$$M_{comp} = F_{steel} \frac{D}{2} + F_{conc} \frac{d_p}{2} - \frac{(F_{steel} - F_{conc})^2 T}{F_{flange} 4} \quad (9)$$

For composite beam with partial shear interaction, F_{con} is less than the smaller of F_{conc} or F_{steel} . The calculated ultimate moment capacity of the composite beam is given by:

$$M_{comp} = M_s + F_{con} \times \left(d_p - \frac{F_{con} d_p}{F_{conc}} \right) - \frac{(F_{steel} - F_{con})^2 T}{F_{flange} 4} \quad (10)$$

Table 4 shows the ultimate moment capacity obtained from rigid - plastic analyse and compared with the results obtained from the present FE solution. Results showed good agreement between the FE solution and the rigid - plastic analysis using the effective width obtained from the FE models.

7. Conclusions

This paper presents a numerical study to determine the effective width of composite beams with precast hollowcore slabs. The model takes into account the non-linear load-slip characteristics of headed stud shear connector and all the other materials non-linearity.

From the parametric study carried out on the effective width of composite beams with hollowcore slabs, it is found that:

1. The effective width is equal to 0.22 L for slab width/span ratio greater or equal to 0.26.
2. For b/L less than 0.26, the effective width can be obtained from Fig. 13.

Moment vs. mid-span deflection curves were plotted using the predicted effective width and the ultimate moment capacity; the modes of failure were also evaluated. Predictions of the ultimate moment capacity obtained from present FE analysis were compared with that of the rigid - plastic analysis. The comparison shows good agreement between both FE solution and the theoretical calculations.

Acknowledgements

The authors would like to acknowledge the support provided by the Egyptian Government, Bison Concrete Products Ltd., Severfield-Reeve Plc. and the skilled assistance provided by the technical staff in the School of Civil Engineering at the University of Leeds.

References

- ABAQUS (1998), User's Manual, Ver. 5.8, Hibbitt, Karlson and Sorensen, Inc.
- Amadio, C. and Fragiocomo, M. (2002), "Effective width evaluation for steel-concrete composite beams", *J. Constructional Steel Research*, **58**, 373-388.
- Ansourian, P. (1975), "An application of the method of finite elements to the analysis of composite floor systems", *Proc. Instn. Civ. Engrs.*, Part 2, Issue 59, 699-726.
- BS 8110 (1997): Parts 1,2, Structural Use of Concrete, "Code of Practice for Design and Construction", British Standards Institution, London.
- EC4 (1994), DD ENV 1994-1-1, "Design of Composite Steel and Concrete Structures. Part 1.1, General Rules and Rules for Buildings (with U.K National Application Document)", British Standards Institution, London.
- El-Lobody, E. and Lam, D. (2002), "Modelling of headed stud in steel - precast composite beams", *Steel and Composite Structures*, **2**(5), 355-378.
- El-Lobody, E. and Lam, D. (2003), "Finite element analysis of steel-concrete composite girders", *Advances in Struct. Eng. – An Int. J.*, **6**(4), 267-281.
- Heins, C.P. and Fan, H.M. (1976), "Effective composite beam width at ultimate load", *J. Struct. Div.*, ASCE, **102**(ST11), 12538-2179.
- Lam, D., Elliott, K.S. and Nethercot, D.A. (2000a), "Experiments on composite steel beams with precast concrete hollow core floor slabs", *Proc. of the Institution of Civil Engineers, Structures and Buildings*, **140**, 127-138.
- Lam, D., Elliott, K.S. and Nethercot, D.A. (2000b), "Designing composite steel beams with precast concrete-hollow core slabs", *Proc. of the Institution of Civil Engineers, Structures and Buildings*, **140**, 139-149.